Energy Storage Materials 37 (2021) 556–566

Contents lists available at ScienceDirect

Energy Storage Materials

journal homepage: www.elsevier.com/locate/ensm

A seawater battery with desalination capabilities enabling a dual-purpose aqueous energy storage system

Do-Hwan Nam, Margaret A. Lumley, Kyoung-Shin Choi*

Department of Chemistry, University of Wisconsin–Madison, Madison, Wisconsin 53706, United States.

ARTICLE INFO

Keywords:
Energy storage systems
Seawater batteries
Na-ion batteries
Desalination

ABSTRACT

Effectively storing electricity produced from renewable sources and increasing the supply of fresh water with a reduced carbon footprint are two pressing issues to sustainably and reliably provide electricity and clean water. In this study, a new aqueous rechargeable Na-ion battery system, which can store/release energy while operating in seawater and can also perform membrane-free seawater desalination, is developed enabling a dual-purpose energy storage system (ESS). The discharging cell of this system is composed of a sodiated $NaTi_2(PO_4)_3$ electrode and a desodiated nickel hexacyanoferrate (NiHCF) electrode in 0.6 M NaCl, and generates an average output voltage of 1.19 V. The charging process is achieved in two separate cells that require low input voltages. In the first, a desodiated $NaTi_2(PO_4)_3$ electrode is paired with Bi as a Cl-storage electrode, and this cell performs desalination during charging. In the second, a sodiated NiHCF electrode is paired with a chlorinated Bi electrode, and this cell performs salination during charging. The energy output generated by the discharging cell is ~94% of the combined energy inputs required by the two charging cells. As the energy consumed for the desalination and salination processes is not truly consumed but rather stored in the system through the charging process, and the majority of the energy stored during charging is recovered during discharging, the extra energy consumed for desalination is minimized. The high energy efficiency and desalination performance of the proof-of-concept dual-purpose ESS are reported with excellent cyclabilities of all component electrodes (> 1000 cycles).

1. Introduction

Concerns about the negative environmental impacts of fossil fuels and an increase in global energy demands have inspired the development of technologies that utilize renewable energy sources such as solar, wind, and tidal to produce green electricity [1]. However, the intermittent nature of renewable energy sources necessitates integration of these technologies with energy storage systems (ESSs) [2–4]. ESSs can store electricity during times of excess electricity production and can then release that electricity in times of high energy demand. Integration of renewable energy technologies and ESSs allows for the development of a robust and reliable electricity system [5,6].

Li-ion batteries (LIBs) are presently one of the most advanced technologies for ESSs due to their high energy density, long cycle life, and excellent energy efficiency [7–10]. However, the high cost, performance reliability, and safety of LIBs are challenges that still need to be addressed for LIBs to be used in large-scale ESSs [10–14]. Recently, aqueous rechargeable Na-ion batteries (ARNBs) have emerged as a promising alternative energy storage solution [11–13]. In general, Na-ion batteries are less expensive than Li-ion batteries, and the use of an aqueous electrolyte eliminates various issues caused by the use of non-aqueous electrolytes in LIBs; aqueous electrolytes are safer, cheaper, and more environmentally benign than non-aqueous electrolytes [14,15]. Aqueous electrolytes also enable higher ionic conductivities than non-aqueous electrolytes [11,12]. One disadvantage of ARNBs is a relatively low cell voltage that is inevitably restricted by the water reduction and oxidation potentials. However, if the advantages offered by ARNBs can be practically realized at a large scale, the merits of ARNBs may outweigh this limitation to make ARNBs a viable candidate for ESSs.

In this study, we present a new ARNB system that can operate in seawater and can also achieve seawater desalination, which drastically increases the benefits offered by ARNBs to make ARNBs more attractive candidates for ESSs. This new ARNB system combines the advantages of ARNBs and desalination batteries. Desalination batteries are rechargeable batteries that consist of a Na-storage electrode and a Cl-storage electrode [16,17]. The charging and discharging processes in desalination batteries are coupled with the removal and release of Na^+ and Cl^- [16–25]. The Na-storage and Cl-storage electrodes used in desalination batteries store Na^+ and Cl^- in the bulk of the electrodes through the formation of chemical bonds, which increases the salt removal capacity relative to capacitive deionization (CDI) [16–27]. Because desalination batteries are rechargeable batteries, they can also store energy during

* Corresponding author.
E-mail address: kschoi@chem.wisc.edu (K.-S. Choi).

https://doi.org/10.1016/j.ensm.2021.02.037
Received 22 October 2020; Received in revised form 30 January 2021; Accepted 21 February 2021
Available online 23 February 2021

charging. However, the output voltage generated by desalination batteries during discharging is typically lower than that of ARNBs [16,17,28]. This is because the chlorination potential of the Cl-storage electrode typically lies between the sodiation potentials of the two Na-storage electrodes chosen to maximize the output voltage of ARNBs [16,17,28]. The low output voltage is not a problem for desalination batteries because the primary purpose of desalination batteries is not to maximize the output voltage but to achieve desalination with a minimum energy input [28]. However, the low output voltage will prevent the use of desalination batteries as efficient ESSs.

In the new ESS demonstrated in this study, a seawater ARNB was constructed to achieve a maximum output voltage during discharging. The charging process was performed in two separate cells that use the desalination and salination reactions to store energy with a low input voltage. During the discharging process, the ARNB discharging cell generates an output voltage that is the sum of the input voltages of the two charging cells, which is much greater than the output voltage that can be generated by traditional desalination batteries. We note that the charging process that requires an energy input is a necessary step for any battery to enable energy storage. As the energy consumed for the desalination and salination processes is not truly consumed but rather stored in the system through the charging process, and the majority of the energy stored during charging is recovered during discharging, the extra energy consumed for desalination is minimized. The new ARNB system presented in this study provides a dual-purpose ESS that can operate using seawater as the electrolyte and generates both electricity and desalinated water as useful products.

2. Results and Discussion

2.1. Operating Principles

Our system uses two Na-storage electrodes and one Cl-storage electrode to construct two charging cells and one discharging cell. Charging Cell 1 is composed of NASICON-type $NaTi_2(PO_4)_3$ [29–32] as the Na-storage electrode and Bi [17,24,33,34] as the Cl-storage electrode (Fig. 1a). In this cell, Na-storage by $NaTi_2(PO_4)_3$ and Cl-storage by Bi occur through the following reactions to achieve desalination:

Cathode reaction:

$$3/2NaTi_2(PO_4)_3 + 3Na^+ + 3e^- \rightarrow 3/2Na_3Ti_2(PO_4)_3 \quad (1)$$

Anode reaction:

$$Bi + Cl^- + H_2O \rightarrow BiOCl + 2H^+ + 3e^- \quad (2)$$

In Charging Cell 1, the cathode potential (sodiation potential of $NaTi_2(PO_4)_3$) is more negative than the anode potential (chlorination potential of Bi), which means that the cell voltage (E_{cell}, $E_{cell} = E_{cathode} - E_{anode}$) is negative (Fig. 1d). Thus, the overall reaction is non-spontaneous and requires an energy input, equivalent to charging. During operation of the cell, Na^+ and Cl^- are removed from seawater that is used as the feedwater and so Charging Cell 1 is also a desalination cell. Because the removal of Na^+ and Cl^- in the desalination charging cell occurs through ion-specific electrode reactions, desalination is achieved without the use of a membrane. We note that reverse osmosis (RO) and other electrochemical desalination methods (e.g. electrodialysis) are based on the use of a membrane, and extra procedures and treatment steps are required to alleviate membrane fouling [35,36].

Charging Cell 2 is composed of a sodiated nickel hexacyanoferrate (NiHCF) electrode and a chlorinated Bi electrode, BiOCl (Fig. 1b). NiHCF is a type of Prussian Blue Analogue (PBA) with the nominal formula $A_xMFe(CN)_6 \cdot nH_2O$ (A: alkali metal ion, M: divalent transition metal ion, $1 \leq x \leq 2$) [38–41]. In this cell, Cl^- is released from BiOCl through the reverse reaction of Eq. 2 (Eq. 3), and Na^+ is released from NiHCF (Eq. 4).

Cathode reaction:

$$BiOCl + 2H^+ + 3e^- \rightarrow Bi + Cl^- + H_2O \quad (3)$$

Anode reaction:

$$3Na_2NiFe^{II}(CN)_6 \rightarrow 3NaNiFe^{III}(CN)_6 + 3Na^+ + 3e^- \quad (4)$$

In this cell, the cathode potential (dechlorination potential of BiOCl) is more negative than the anode potential (desodiation potential of Ni-HCF), which means that E_{cell} is negative (Fig. 1e). Thus, the overall reaction is non-spontaneous and requires an energy input, equivalent to charging. Because Na^+ and Cl^- are released into the feedwater during the cell reaction, Charging Cell 2 is also a salination cell.

Discharging Cell is composed of a sodiated $NaTi_2(PO_4)_3$ electrode and a desodiated NiHCF electrode. In this cell, Na^+ will be released from $NaTi_2(PO_4)_3$ (reverse reaction of Eq. 1) and inserted into NiHCF (reverse reaction of Eq. 4). In this cell, the cathode potential (sodiation potential of NiHCF) is more positive than the anode potential (desodiation potential of $NaTi_2(PO_4)_3$), which means that E_{cell} is positive (Fig. 1f). Thus, the overall reaction is spontaneous and generates an energy output, equivalent to discharging. As the desodiation potential of $NaTi_2(PO_4)_3$ is very close to the water reduction potential, and the sodiation potential of NiHCF is very close to the water oxidation potential, the combination of these two electrodes enables the generation of the maximum output voltage allowed for ARNBs. When the discharging process is complete, the desodiated $NaTi_2(PO_4)_3$ electrode can be used in Charging Cell 1, and the sodiated NiHCF electrode can be used in Charging Cell 2 to allow for repeated charging and discharging cycles.

In a typical ARNB, the same two electrodes are used for both discharging and charging, and the input voltage required for charging is comparable to the output voltage generated during discharging. In our new system, rather than combining $NaTi_2(PO_4)_3$ and NiHCF to perform the charging process, the charging process is divided and performed in two separate cells. In the charging cells, $NaTi_2(PO_4)_3$ and NiHCF are each combined with Bi/BiOCl that has a chlorination/dechlorination potential that lies between the sodiation/desodiation potentials of $NaTi_2(PO_4)_3$ and NiHCF. This new cell design provides two major advantages. First, while the typical charging process is used only to store energy, in our new design the two charging cells perform desalination (Charging Cell 1) and salination (Charging Cell 2) concurrently with energy storage. As a result, our new device achieves desalination during charging and generates electricity during discharging. We note that all conventional desalination methods (distillation, RO, electrodialysis) always consume energy to convert the feedwater to desalinated water and have no ability to store energy. Second, the input voltages required for the charging process of Charging Cell 1 and Charging Cell 2 are approximately half of the input voltage that would be required to charge the cell composed of $NaTi_2(PO_4)_3$ and NiHCF electrodes. While the total energy required to charge the system does not change, the use of charging cells that require a lower input voltage may allow these cells to utilize a greater fraction of renewable electricity with fluctuating power. These two advantages increase the efficacy of the proposed ARNB system and make it a highly attractive novel candidate for ESSs.

2.2. Enhanced Cyclability of Electrodes Enabled by New Fabrication Method

While our new ARNB system is conceptually plausible, it cannot be considered as a practically viable ESS unless all the component electrodes exhibit long-term cyclability. The long-term cyclability of the Bi electrode is of a particular concern. This is because, unlike $NaTi_2(PO_4)_3$ and NiHCF that achieve sodiation through intercalation with a minimal structural change of the host material, chlorination of Bi results in a 158% volume expansion, forming a different phase, BiOCl (Fig. S1) [17]. Therefore, repeated conversion between Bi and BiOCl can result

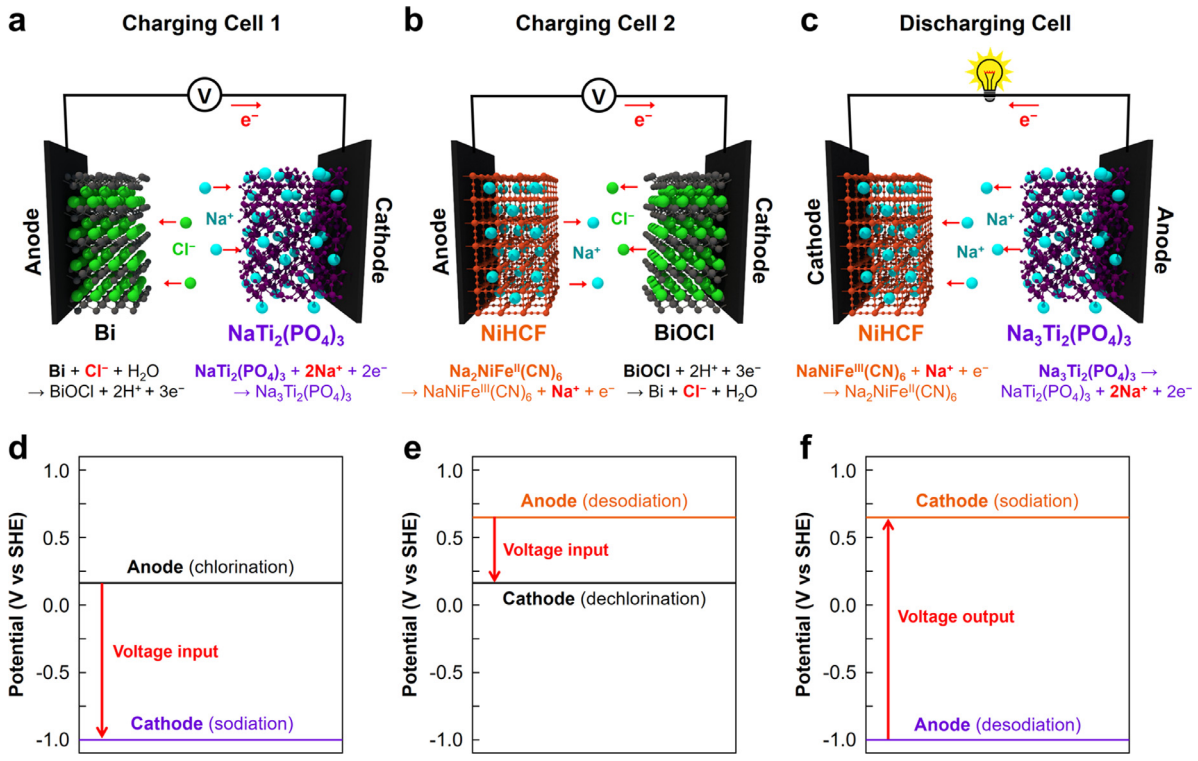

Fig. 1. A schematic diagram illustrating the operation of (a) Charging Cell 1, (b) Charging Cell 2, and (c) Discharging Cell with the expected cathode and anode potentials for (d) Charging Cell 1, (e) Charging Cell 2, and (f) Discharging Cell.

in degradation of the electrode. However, Bi is the most practical candidate for use as a large-scale Cl-storage electrode reported to date because of its relatively low cost, high specific capacity of 384.75 mAh g^{-1} (Cl-storage capacity = 169.6 mg_{Cl}/g_{Bi}), exceptional stability in a wide range of pH conditions, and high Faradaic efficiency for Cl^- removal [17,24,33,34]. Previously, we demonstrated that an electrodeposited Bi foam electrode could be cycled 200 times [17], which is not sufficient to seriously consider the use of Bi electrodes for a practical ESS. Thus, we invested a significant amount of effort to develop a new fabrication method to enable long-term cyclability of Bi electrodes.

Our new fabrication method involves the preparation of Bi electrodes as sheet-type electrodes. In this process, a high-energy ball mill is used to mix Bi powder with a conductive carbon agent. A polytetrafluoroethylene (PTFE) binder is then added to the Bi/carbon mixture and a rolling-pressing procedure is used to fabricate sheet-type electrodes. Unlike commercial battery electrodes that are manufactured by casting a slurry onto a metallic current collector, sheet-type electrodes are flexible and mechanically robust (Fig. 2a); they can bend without cracking or delaminating from a current collector. In the sheet-type electrode, individual Bi particles are encapsulated by carbon and binder coating layers (Fig. 2b). In the nanocrystalline Bi foam electrode that we reported previously, pulverization results in the formation of disintegrated particles, which are mechanically detached from the electrode, resulting in capacity fading [17]. However, in this new sheet-type electrode, individual Bi particles are surrounded by a 3D network of carbon and binder, and so even if disintegrated sub-particles are formed by pulverization, they still remain within the encapsulated region. Therefore, as long as the Bi particles remain in contact with the conductive carbon, they can still participate in electrochemical reactions, which alleviates capacity fading.

Another effective strategy that we employed to increase the cyclability of Bi was to use Bi_2O_3 particles instead of Bi particles to fabricate the aforementioned sheet-type electrodes. We hypothesized that the encapsulation method would work best if the encapsulation layer is formed when the electrochemically active species is at its greatest volume (i.e. BiOCl rather than Bi). This strategy ensures that sufficient volume is secured within the encapsulated area so that the encapsulating layer does not need to further expand during cycling, minimizing possible structural damage. However, when we used BiOCl particles instead of Bi particles in our fabrication process, we found that the quality of the adhesion between the carbon and BiOCl particles was not as good as that between the carbon and Bi particles. Therefore, the use of BiOCl particles did not result in a notable enhancement in the cyclability. Thus, we used Bi_2O_3 particles instead of BiOCl particles to prepare our sheet-type electrodes; the volume of Bi_2O_3 is larger than that of Bi by 135%, and the use of Bi_2O_3 results in good adhesion with carbon (Fig. S1-2). Furthermore, commercial Bi_2O_3 is significantly cheaper than commercial BiOCl and will be more compatible with the large-scale fabrication of Bi electrodes. After electrode fabrication, the resulting sheet-type Bi_2O_3 electrodes were first electrochemically reduced to Bi. The Bi electrodes were then used for the conversion between Bi and BiOCl through chlorination and dechlorination (Fig. S3).

Another important strategy that we used to achieve maximum cyclability of Bi was not to completely convert Bi to BiOCl during the cycling test. Instead, we chose to use only ~33% of the Bi for electrochemical reactions, and the remaining Bi was used to maintain the structural integrity of the electrode. During chlorination, the formation of BiOCl begins at the Bi/electrolyte interface, and the Bi/BiOCl phase boundary moves from the Bi/electrolyte interface toward the Bi/carbon interface (Fig. 2c-d). Therefore, by limiting the capacity during the cycling tests, the Bi at the Bi/carbon interface can remain as Bi to maintain good electrical contact to carbon. If full conversion of Bi is used during the cycling tests, while the Bi directly bound to carbon is transformed to BiOCl, the Bi/carbon contact can become loose or get damaged, resulting in the formation of electrochemically isolated Bi/BiOCl particles that ultimately causes capacity fading.

The cyclabilities of the sheet-type Bi electrodes tested using 100% and ~33% of the capacity of Bi are compared in Fig. 3a-d. The cyclabil-

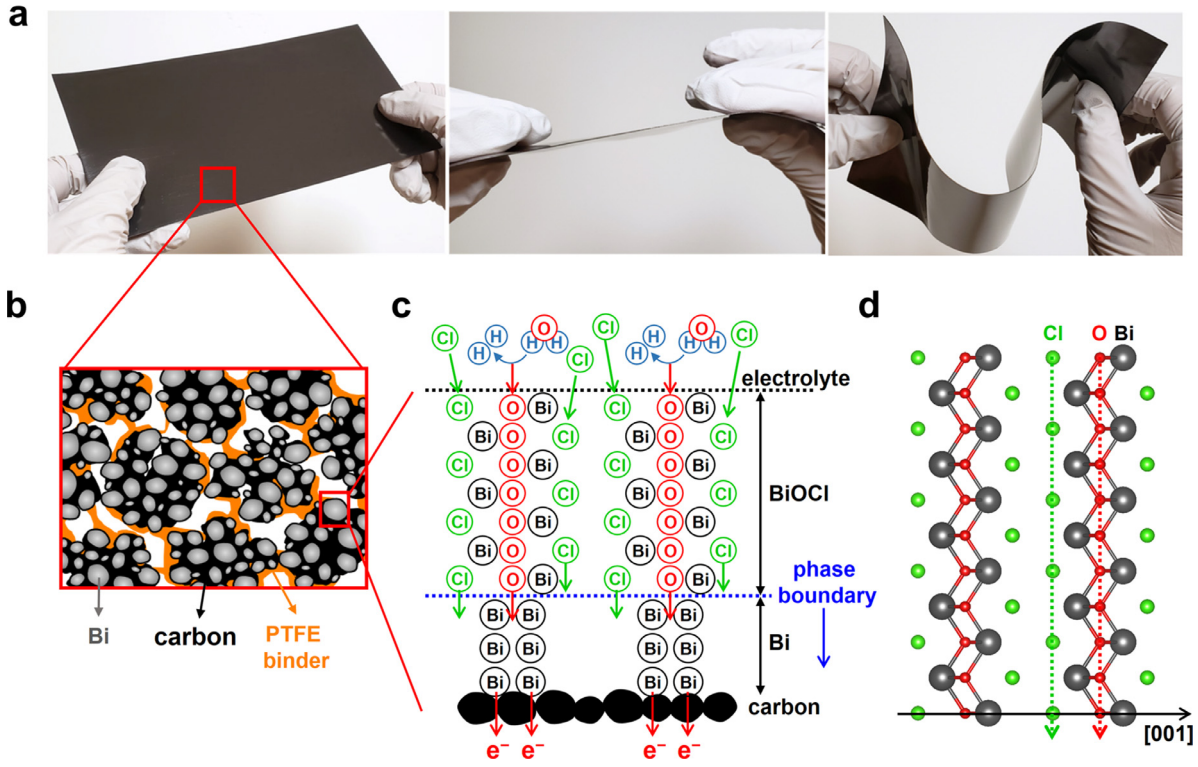

Fig. 2. (a). Photographs of a sheet-type Bi electrode and (b) a schematic illustration of the structure of the sheet-type Bi electrode. (c) A diagram depicting the growth of BiOCl upon oxidation of Bi through the insertion of Cl^- and O^{2-} into the Bi lattice. The Bi/BiOCl phase boundary moves from the Bi/electrolyte interface toward the Bi/carbon interface. (d) Crystal structure of BiOCl composed of 2D BiOCl layers stacked perpendicular to the [001] direction. The movement of Cl^- and O^{2-} can readily occur along directions perpendicular to the [001] direction.

ity of the Bi electrode was evaluated in 0.6 M NaCl, an electrolyte that mimics the salinity of seawater. The Bi electrodes were cycled galvanostatically at a current density of ± 4 mA cm^{-2} (~1.5 C-rate) with cutoff potentials of 0.7 V and −1.45 V vs Ag/AgCl for chlorination and dechlorination, respectively. The potential-capacity plots obtained using 100% of the capacity of the Bi electrode are shown in Fig. 3a. The initial chlorination and dechlorination capacities were 283.70 and 306.85 mAh g^{-1}, respectively. The average potentials observed during chlorination and dechlorination were 0.08 V and −0.78 V vs Ag/AgCl, respectively. XRD patterns confirmed the formation of BiOCl after chlorination and the disappearance of BiOCl after dechlorination (Fig. S3). The change in the chlorination capacity over 1200 cycles is shown in Fig. 3b. The chlorination capacity after 200 cycles was 268.13 mAh g^{-1}, corresponding to a capacity retention of 94.5%. This is a remarkable improvement compared with the performance of the previously reported electrodeposited Bi foam electrode, which maintained only ~60% of its initial capacity after 200 cycles [17]. The improvement in cyclability clearly demonstrates the advantage of our new fabrication method. However, after 200 cycles the capacity of the sheet-type Bi electrode decreased gradually, and after the 1114^{th} cycle the capacity dropped below 100 mAh g^{-1}. The average Coulombic efficiency throughout the cycling test was ~104 %.

When the chlorination capacity was restricted to 100 mAh g^{-1} (~33% of the full capacity), a capacity of 100 mAh g^{-1} was maintained for 7200 cycles with no decrease in performance (Fig. 3c-d). Also, comparing the accumulated capacity of the Bi electrodes before the capacity of Bi drops below 100 mAh g^{-1} (shaded areas in Fig. 3b and 3d) reveals that the Bi electrode cycled with a restricted capacity has an accumulated capacity that is 3.4 times larger than that of the Bi electrode cycled with its full capacity. This performance is remarkable and clearly illustrates the advantage of restricting the capacity of the Bi electrode to 100 mAh g^{-1} to increase the electrode lifetime. When the Bi electrode operates with a restricted capacity, the Bi that does not participate in the electrochemical reactions should not necessarily be considered as capacity that is not fully utilized but rather as an inexpensive conductive and structural component of the electrode. The rational design of electrode fabrication and operational conditions presented here enabled the use of Bi electrodes for more than 7000 cycles with no loss in performance, allowing us to consider the use of Bi for practical ESS and desalination applications.

Inspired by such a remarkable improvement in the lifetime of Bi enabled by our new fabrication method, $NaTi_2(PO_4)_3$ was also fabricated as a sheet-type electrode following the same procedure. Detailed synthesis conditions and structural characterization of $NaTi_2(PO_4)_3$ powder, as well as the electrode fabrication procedure can be found in the experimental section and SI (Fig. S4-S5). The cycle performance of the sheet-type $NaTi_2(PO_4)_3$ electrode was investigated in 0.6 M NaCl at a current density of ± 2 mA cm^{-2} (~1.5 C-rate) with cutoff potentials of −0.93 V and −0.2 V vs Ag/AgCl for sodiation and desodiation, respectively. The potential-capacity plots obtained during sodiation and desodiation are shown in Fig. 3e and agree well with those reported in previous studies of $NaTi_2(PO_4)_3$ [31,32]. The average potentials observed during sodiation and desodiation were −0.83 V and −0.71 V vs Ag/AgCl, respectively.

The change in the sodiation capacity over 1000 cycles is shown in Fig. 3f. The initial sodiation capacity of the $NaTi_2(PO_4)_3$ electrode was 66.83 mAh g^{-1} and it decreased slightly to 56.85 mAh g^{-1} after 1000 cycles, corresponding to a capacity retention of 85.1%, with a Coulombic efficiency of 93.5% throughout the test. This is a remarkable improvement in the cycle performance of $NaTi_2(PO_4)_3$ in 0.6 M NaCl. In our previous study we prepared a $NaTi_2(PO_4)_3$ electrode by mixing $NaTi_2(PO_4)_3$ powder with a conductive carbon additive and PTFE binder by hand in a mortar and pestle, and demonstrated only 50 sodiation/desodiation cycles (94.2% capacity retention) [17]. It appears that

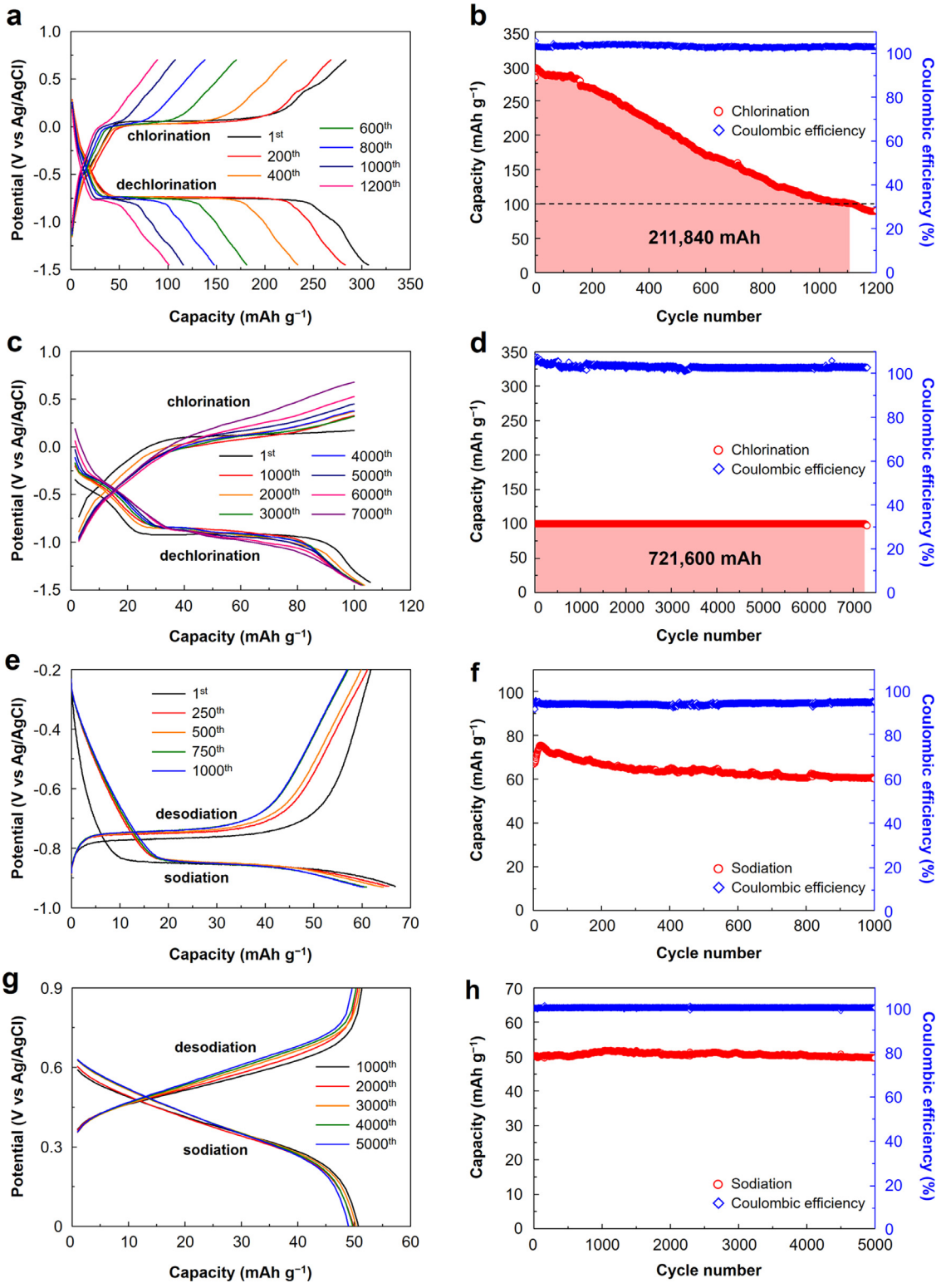

Fig. 3. (a). Potential-capacity plots and (b) cyclability and Coulombic efficiency of the Bi electrode at ± 4 mA cm^{-2} in 0.6 M NaCl with cutoff potentials of −1.45 V and 0.7 V vs Ag/AgCl. (c) Potential-capacity plots and (d) cyclability and Coulombic efficiency of the Bi electrode when the chlorination capacity was restricted to 100 mAh g^{-1}. (e) Potential-capacity plots and (f) cyclability and Coulombic efficiency of the $NaTi_2(PO_4)_3$ electrode in 0.6 M NaCl at ± 2mA cm^{-2} with cutoff potentials of −0.93 V and −0.2 V vs Ag/AgCl. (g) Potential-capacity plots and (h) cyclability and Coulombic efficiency of the NiHCF electrode in 0.6 M NaCl at ± 4 mA cm^{-2} with cutoff potentials of 0.0 V and 0.9 V vs Ag/AgCl.

the use of a high-energy ball mill allowed for more uniform and intimate carbon coating of the $NaTi_2(PO_4)_3$ particles. The rolling-pressing procedure also facilitated better contact between carbon-coated $NaTi_2(PO_4)_3$ particles within the electrode, resulting in the formation of high-quality electrodes that demonstrated good cyclability. With further optimization, we believe that the lifetime of $NaTi_2(PO_4)_3$ can be further improved.

NiHCF was also fabricated as a sheet-type electrode using the same procedure. Detailed synthesis conditions and structural characterization of NiHCF powder, as well as the electrode fabrication procedure can be found in the experimental section and SI (Fig. S6-S7, Table S1). The cycle performance of the sheet-type NiHCF electrode was investigated in 0.6 M NaCl at a current density of ± 4 mA cm^{-2} (~6 C-rate) with cutoff potentials of 0.0 V and 0.9 V vs Ag/AgCl for sodiation and desodiation, respectively. The potential-capacity plots obtained during sodiation and desodiation are shown in Fig. 3g. The average potentials observed during sodiation and desodiation were 0.36 V and 0.56 V vs Ag/AgCl, respectively.

The long-term cycle performance of the NiHCF electrode is shown in Fig. 3f. The initial sodiation capacity of the NiHCF electrode was 50.25 mAh g^{-1} and the sodiation capacity after 5000 cycles was 49.6 mAh g^{-1}, corresponding to a capacity retention of 98.7% (Fig. 3f). Furthermore, the NiHCF electrode demonstrated an impressive Coulombic efficiency of 99.8% throughout the cycling test. A Coulombic efficiency near 100% illustrates the highly reversible redox properties of NiHCF and indicates that no parasitic side reactions or irreversible phase transitions occur during the cycling test. The cycle performance of NiHCF shown here is a significant improvement compared with the cycle performance of NiHCF reported in our previous study [41]. In this previous study, the NiHCF electrode was prepared by mixing NiHCF powder with a conductive carbon additive and PTFE binder by hand in a mortar and pestle, and the capacity retention of this electrode after 200 cycles was 95%. The improved performance demonstrated by sheet-type NiHCF electrodes again highlights the advantages of our new processing method.

The results presented in this section show that the electrodes chosen for our new electrochemical system can serve as practical component electrodes for our dual-purpose ARNB. We believe that the cyclability of the electrodes shown here can be further improved by continued optimization of the electrode fabrication process. In the next section, we will describe how these electrodes can be used to construct a combined desalination/ARNB system, and we will examine the energy storage and desalination capabilities of the system.

2.3. Operation of Charging and Discharging Cells

The energy storage and release processes and the desalination performance of the aqueous rechargeable system combining Bi, $NaTi_2(PO_4)_3$, and NiHCF electrodes were investigated galvanostatically. During the cell operation, the individual potentials of the anode and cathode were monitored against an Ag/AgCl reference electrode.

The performance of Charging Cell 1 composed of Bi and $NaTi_2(PO_4)_3$ electrodes was investigated in 0.6 M NaCl at a current density of 1.33 mA cm^{-2} (~0.5 C-rate based on the Bi electrode) until the capacity of the Bi electrode reached 100 mAh g^{-1} (Fig. 4a). The individual potential profiles show that the reduction of $NaTi_2(PO_4)_3$ (sodiation/cathode) occurs at −0.807 V vs Ag/AgCl while the oxidation of Bi to BiOCl (chlorination/anode) occurs at −0.067 V vs Ag/AgCl. Thus, the average input voltage required to operate Charging Cell 1 is 0.74 V. Charging Cell 1 also removed Na^+ and Cl^- from the electrolyte to achieve desalination.

The performance of Charging Cell 2 composed of Bi and NiHCF electrodes was examined in an acidic solution containing 70 mM HCl (pH 1.3). The use of an acidic solution was necessary to improve the dechlorination kinetics of BiOCl [17,24,33,34], and therefore decrease the input voltage required to operate Charging Cell 2. In our previous study we thoroughly investigated the electrochemical properties of Bi and found that while the chlorination kinetics of Bi are fast in neutral solutions, the dechlorination kinetics of BiOCl are slow and require a large overpotential in neutral solutions. This is because dechlorination of BiOCl involves the release of both Cl^- and O^{2-} from the BiOCl lattice (reverse of Fig. 2c). We discovered that the use of an acidic electrolyte where H^+ can serve as an O^{2-} acceptor can drastically reduce the overpotential required for the reduction of BiOCl (Fig. S8). (Detailed overpotential analyses for the conversion between Bi and BiOCl using linear sweep voltammograms can be found in our previous study [17].) While Charging Cell 1 is designed to achieve seawater desalination and must use seawater as the feedwater, Charging Cell 2 is designed to regenerate the Bi electrode and does not need to use seawater as the feedwater; the choice of electrolyte for Charging Cell 2 is flexible. Therefore, an acidic electrolyte was used to minimize the energy input required for Charging Cell 2. (Acidic wastewater or acidified seawater can be used for the practical implementation of Charging Cell 2.)

Other than the electrolyte type, the performance of Charging Cell 2 was investigated with the same operating conditions as Charging Cell 1 (Fig. 4b). The individual potential profiles show that the reduction of BiOCl to Bi (dechlorination/cathode) occurs at −0.147 V vs Ag/AgCl on average while the oxidation of NiHCF (desodiation/anode) occurs at 0.367 V on average, indicating that the Bi/NiHCF cell requires an average input voltage of 0.514 V (Fig. 4b).

The performance of Discharging Cell composed of NiHCF and $NaTi_2(PO_4)_3$ electrodes was investigated in 0.6 M NaCl at a current density of 1.33 mA cm^{-2}. The individual potential profiles show that the reduction of NiHCF occurs at 0.41 V (sodiation/cathode) on average while the oxidation of $NaTi_2(PO_4)_3$ occurs at −0.78 V (desodiation/anode) on average, resulting in an average output voltage of 1.19 V. Considering that the thermodynamic electrochemical stability window of aqueous electrolytes is 1.23 V due to the occurrence of water oxidation and water reduction, the output voltage reported here approaches the thermodynamic limit. Therefore, the combination of NiHCF and $NaTi_2(PO_4)_3$ electrodes is suitable to construct an ANRB with a maximum output voltage. The fact that this cell is truly a discharging cell and can generate electricity was visually demonstrated by connecting the cell to a small LED bulb. The LED bulb was illuminated when the NiHCF and $NaTi_2(PO_4)_3$ electrodes were simply immersed in seawater (no external electrical energy was supplied) (Fig. S9).

The energy efficiency of the system (energy output divided by energy input, multiplied by 100%) was examined by dividing the output energy generated by Discharging Cell by the sum of the input energies required to operate Charging Cells 1 and 2. The energy output and inputs required for the electrochemical reactions were calculated by integrating the areas between the cell voltage (the difference between the cathode and anode potentials) and capacity plots (the shaded regions in Fig. 4a-c). We note that the capacities of the three cells were slightly different (100 mAh g_{Bi}^{-1} for Charging Cell 1, 105.29 mAh g_{Bi}^{-1} for Charging Cell 2, and 105.36 mAh g_{Bi}^{-1} for Discharging Cell) (Fig. S10a-c). This is because the Coulombic efficiency of the Bi electrode is slightly higher than 100% (Fig. 3d) (i.e. the dechlorination capacity is slightly greater than the chlorination capacity). A detailed explanation of the effect of this phenomenon on the capacities of the three cells is provided in the experimental section. When the as-obtained potential-capacity plots of Charging Cells 1 and 2 and Discharging Cell were used to calculate the energy efficiency of the system, the energy efficiency was overestimated (~99%) (Fig. S10d). In order to obtain a more accurate energy efficiency, we normalized the capacities of all three cells to be identical (100 mAh). With the potential-normalized capacity plots shown in Fig. 4a, the energy inputs required for Charging Cell 1 and Charging Cell 2 were calculated to be 74.10 mW and 51.44 mW, respectively, giving a total energy input of 125.54 mW. The energy output generated by Discharging Cell was calculated to be 118.73 mW. Therefore, the energy efficiency of the system was found to be 94.6% for the first cycle. The performance of the complete system was monitored for 15 consecutive cycles, and the energy input and output showed negligible changes throughout the duration of the test to give an average

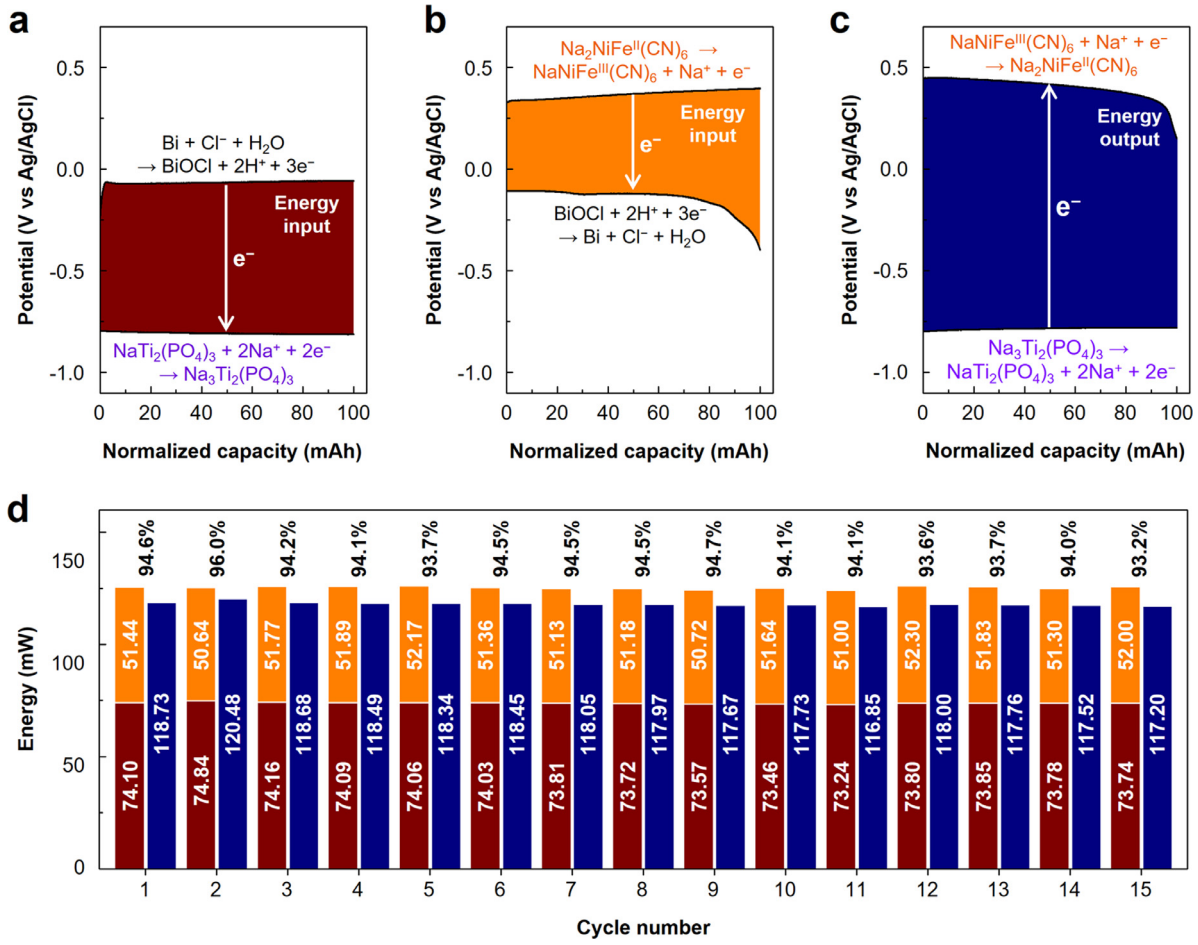

Fig. 4. Normalized potential-capacity plots obtained at 1.33 mA cm^{-2} for (a) Charging Cell 1 (the Bi/$NaTi_2(PO_4)_3$ cell) in 0.6 M NaCl, (b) Charging Cell 2 (the NiHCF/Bi cell) in 70 mM HCl (pH 1.3), and (c) Discharging Cell (the NiHCF/ $NaTi_2(PO_4)_3$ cell) in 0.6 M NaCl. (The capacities of all three cells were normalized to be 100 mAh.) The individual potentials of the electrodes were measured against an Ag/AgCl RE. (d) The energy inputs required for Charging Cell 1 (brown) and Charging Cell 2 (orange), the energy output generated by Discharging Cell (blue), and the energy efficiency obtained for 15 cycles.

energy efficiency of 94.2%. The energy efficiency demonstrated here is impressive even when we consider the combined system solely as an energy storage device. As the charging cells not only store energy but also achieve desalination/salination, the complete system reported here can achieve desalination with minimal energy consumption.

The cycling test was only reported for 15 cycles because the electrodes and electrolytes were manually switched for tests of the combined system, which is difficult. As the individual electrodes have already exhibited exceptional cyclability, we expect that the combined system will also be able to achieve similar cyclability. In the future, we plan to design a cell that can perform long-term cyclability test without requiring manual switching of the electrodes. Additionally, continued optimization of the individual electrodes will further increase the cyclability of the combined cell. The optimization process will also involve identifying and resolving the factors that cause the electrode Coulombic efficiencies to deviate from 100%.

We note that the solution pH of Charging Cell 1 decreases over time because the conversion of Bi to BiOCl produces H^+ (Eq. 2). Similarly, the solution pH of Charging Cell 2 increases over time because the conversion of BiOCl to Bi consumes H^+ (Eq. 3). For the small-scale electrodes used in this study, the impact of the solution pH changes was not significant. However, when a larger amount of Cl^- is stored and released by larger Bi/BiOCl electrodes, the changes in solution pH may become more pronounced. Thus, it is worthwhile to discuss the potential effects of the solution pH changes on the cell performances. All of the electrodes used in Charging Cells 1 and 2 are chemically stable in acidic media. One possible concern for the operation of Charging Cell 1 in a medium with a decreasing pH is the increasing tendency for the self-discharging reaction of $Na_3Ti_2(PO_4)_3$ (the sodiated form of $NaTi_2(PO_4)_3$) to occur; $Na_3Ti_2(PO_4)_3$ can be spontaneously oxidized to $NaTi_2(PO_4)_3$ by reducing water ($Na_3Ti_2(PO_4)_3 + 2H^+ \rightarrow NaTi_2(PO_4)_3 + 2Na^+ + H_2$), [32,42] which can decrease the Coulombic efficiency of the electrode. If this reaction becomes an issue, optimization of the surface coating of $NaTi_2(PO_4)_3$ particles can be explored to suppress water reduction on $Na_3Ti_2(PO_4)_3$ [42]. One possible concern for the operation of Charging Cell 2 in a medium with an increasing pH is that the dechlorination kinetics of BiOCl decrease as the pH increases, as mentioned previously. Thus, when the solution pH increases, the cell efficiency may decrease slightly. However, considering the impressive energy efficiency demonstrated in this study, a slight decrease in the cell efficiency caused by increasing the size of the electrodes should not considerably affect the practical feasibility and benefits of the new dual-purpose ARNB system.

2.4. Desalination Performance

The Faradaic efficiencies (FEs) for the removal of Na^+ and Cl^- in Charging Cell 1 were evaluated by monitoring the changes in Na^+ and Cl^- concentrations in the electrolyte during the charging process. The concentration changes of Na^+ and Cl^- were determined using a sodium ion meter and chloride ion meter, respectively, after passing a charge of 0, 9, 18, and 27 C (Fig. 5a). The ion-selective electrodes used in the ion meters quantify the ion concentration by measuring the potential dif-

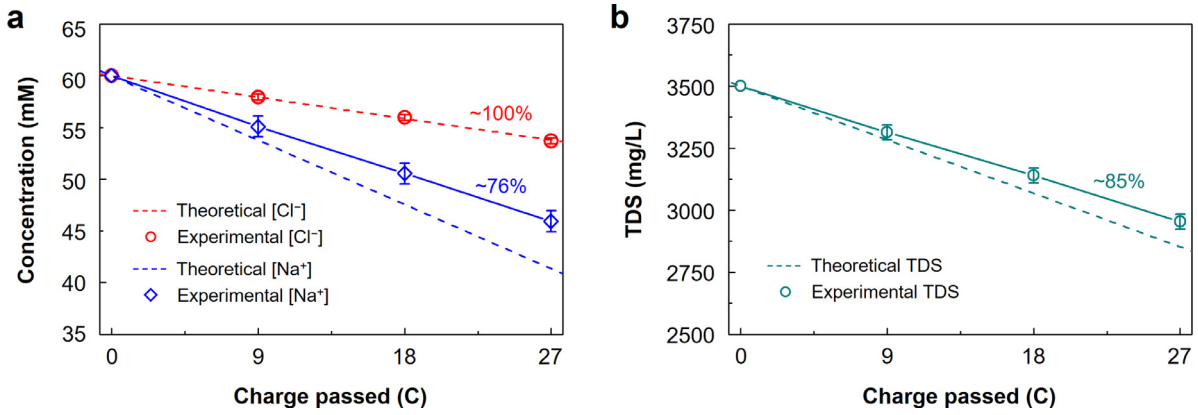

Fig. 5. (a). Change in Na^+ and Cl^- concentrations and (b) change in the concentration of total dissolved solids (TDS) of the electrolyte in the Bi/$NaTi_2(PO_4)_3$ cell after passing a charge of 0, 9, 18, and 27 C.

ference caused by the concentration difference. Due to the logarithmic relationship between concentration and potential from the Nernst equation, a more reliable voltage reading can be obtained when the change in ion concentration exceeds ~10% of the initial concentration. Thus, when the same amounts of Na^+ and Cl^- are removed, a more obvious and reliable difference in the potential reading, and therefore a more accurate determination of the change in Na^+ and Cl^- concentrations, will be obtained when the initial concentration of the solution is low. Therefore, 0.06 M NaCl was used instead of 0.6 M NaCl for this experiment. We emphasize that all other experiments reported in this study were performed using 0.6 M NaCl as the electrolyte, and 0.06 M NaCl was used to calculate the desalination efficiency only to obtain more reliable results from the ion-selective electrodes. According to Le Chatelier's principle (or if the Nernst equation is used to calculate the equilibrium potentials for the Na- and Cl-storage reactions), the Na- and Cl-storage reactions are more favored in 0.6 M NaCl than in 0.06 M NaCl. Thus, we expect that the desalination efficiency in 0.6 M NaCl will be at least as high as that determined using 0.06 M NaCl, which is shown below.

Our results show that the FE of the Bi electrode for Cl^- removal was ~100%, which agrees well with previous results [17,24,33,34]. The high FE of Bi for Cl^- removal is attributed to the fact that there are no other oxidation reactions that can compete with the oxidation of Bi to BiOCl within the cell operating potential region [17]. The FE of the $NaTi_2(PO_4)_3$ electrode for Na^+ removal, on the other hand, was ~76%. The low FE is likely due to the occurrence of a redox reaction between $Na_3Ti_2(PO_4)_3$ and O_2 dissolved in the solution [32]. Overall, Charging Cell 1 was able to decrease the concentration of total dissolved solids (TDS) present in 0.06 M NaCl by ~15% after 27 C of charge were passed (Fig. 5b).

We note that the $NaTi_2(PO_4)_3$/Bi cell removes Na^+ and Cl^- with a 3:1 ratio because Bi requires $3e^-$ to remove one Cl^- (Eq. 2) while $NaTi_2(PO_4)_3$ requires $1e^-$ to remove one Na^+ (Eq. 1). Thus, when 100% of Na^+ present in seawater has been removed by our desalination battery, only 33% of Cl^- will have been removed. The conversion of Bi to BiOCl also results in the production of protons (Eq. 2) [33]. In essence, our desalination cell can convert 0.6 M NaCl to 0.4 M HCl, reducing the ion concentration by 33% with a minimal energy input. We envision that the remaining Cl^- and H^+ can be removed by a successive electrochemical process where Cl^- is converted to Cl_2 gas at the anode and H^+ is converted to H_2 gas at the cathode. These reactions are already used for the well-established chlor-alkali process to produce valuable Cl_2 and H_2 gases [43]. Thus, the construction of a cell to remove the remaining Cl^- and H^+ should not require significant development efforts. In the chlor-alkali process, a highly concentrated NaCl solution (e.g. 4 M NaCl) is used as the feedwater and Cl^- and H^+ are removed in a 1:1 ratio to produce a concentrated NaOH solution. In our proposed process, 0.4 M HCl will be used as the feedwater and will be converted to slightly acidic brackish water. The combination of Charging Cell 1 with subsequent conversion of the product water to mildly acidic brackish water can offer an inexpensive route to convert seawater to brackish water, which then can be converted to fresh water by reverse osmosis (RO) or electrodialysis. (RO or electrodialysis will be used to remove the remaining Cl^- and other ions present in the desalinated water). When brackish water is used as the feedwater, the energy and cost for freshwater production by RO is significantly lower than when seawater is used as the feedwater. For example, the annual electricity cost required to operate a seawater RO (SWRO) plant is more than three times higher than that required for a brackish water (BWRO) plant of the same size [44]. Furthermore, even the construction costs of these two plants are drastically different; an SWRO plant costs more than twice as much to build as a BWRO plant of the same size [44]. Additionally, while the desalination of seawater by electrodialysis is cost-prohibitive, desalination of brackish water by electrodialysis is cost-effective [36].

Thus, we believe that the dual-purpose ARNB demonstrated in this study, which can convert seawater to brackish water with a drastically reduced energy input, will be able to provide more efficient and practical strategies for renewable electricity storage and desalination of seawater.

3. Conclusions

In summary, we have successfully demonstrated the construction of a dual-purpose ESS. The discharging cell used in this system was a high-voltage ARNB composed of a sodiated $NaTi_2(PO_4)_3$ anode and a desodiated NiHCF cathode operating in 0.6 M NaCl. The discharging cell generated an average output voltage (V) of 1.19 V, which is very close to the thermodynamic voltage limit of aqueous batteries (1.23 V). The charging process was achieved in two separate cells, where each of the Na-storage electrodes was paired with a Bi/BiOCl electrode. The charging cell composed of a desodiated $NaTi_2(PO_4)_3$ cathode and a Bi anode also achieved desalination during charging. As the removal of Na^+ and Cl^- in the desalination charging cell occurred through ion-specific electrode reactions, this cell did not require the use of a membrane. The Faradaic efficiencies for Na^+ and Cl^- removal in the desalination charging cell were ~76% and ~100%, respectively. The charging cell composed of a sodiated NiHCF anode and a BiOCl cathode performed salination during the charging process, regenerating the NiHCF and Bi electrodes for subsequent use in the discharging cell and desalination charging cell, respectively. The energy output of the discharging cell was found to be ~94% of the sum of the energy inputs required for the two charging cells. As the energy consumed for the desalination and salination processes is not truly consumed but rather stored in the system through the charging process, and the majority of the energy stored during charging is recovered during discharging, the extra energy consumed for desalina-

tion is minimized. All electrodes used in our dual-purpose ESS exhibited excellent cyclabilities because of the new electrode fabrication methods developed in this study, which can be improved even further with continued optimization efforts. The integration of a high voltage seawater ARNB and desalination/salination cells demonstrated in this study offers a new opportunity to simultaneously address challenges related to renewable electricity storage and seawater desalination.

Compared with typical ARNBs where the electrolyte is held within the battery, our dual-purpose ESS that achieves desalination in addition to energy storage/release will require additional engineering efforts for practical and efficient operation; the desalinated and salinated water need to be replaced after each charging and discharging step. However, the operation of a three-step desalination cell is not much more complex than the operation of a two-step desalination cell. This is because the three-step system does not necessarily require the construction of three physically separate cells, and various engineering approaches can be used to design an efficient and practical system. For example, all three electrodes can be placed in the same container and a different pair of electrodes will be electrically connected depending on the process that will be performed. The container will be filled with a desired electrolyte before each process, and the desalinated or salinated water that is produced will be drained and collected through a designated outlet. Thus, the added complication does not come from the three-step system itself but from the added desalination capability of the cell, which justifies the extra complexity necessary to achieve the additional benefit of simultaneous desalination. The unique advantages provided by the dual-purpose ESS presented in this study, which allows for simultaneous membrane-free desalination and energy storage, considerably increase the benefit of ARNBs and encourage the continued development of this technology.

4. Experimental

4.1. Materials

Bi_2O_3 (99.999%, PURATREM), graphite (99.995%, Sigma-Aldrich), $C_{16}H_{36}O_4Ti$ (97%, Sigma-Aldrich), H_2O_2 (30% solution, EMD Millipore), NH_4OH (28–30% NH_3 basis), $C_6H_8O_7$ (99.0-102.0%, Alfa Aesar), $NH_4H_2PO_4$ (≥98%, Sigma-Aldrich), Na_2CO_3 (Macron), HNO_3 (70%, Sigma-Aldrich), $NiCl_2$•$6H_2O$ (98%, Alfa Aesar), $Na_3C_6H_5O_7$•$2H_2O$ (≥98%, Mallinckrodt), $Na_4Fe(CN)_6$•$10H_2O$ (≥99%, Sigma-Aldrich), polytetrafluoroethylene (PTFE) (60 wt % dispersion in H_2O, Sigma-Aldrich), colloidal graphite (isopropanol, Ted Pella, Inc.), NaCl (99%, Macron), KNO_3 (99.0%, Alfa Aesar) and EtOH (200 proof, Decon Labs Inc.) were used without further purification. Deionized water (Barnstead E-pure water purification system, resistivity >18 MΩ•cm) was used to prepare all solutions.

4.2. Synthesis of $NaTi_2(PO_4)_3$ and NiHCF

$NaTi_2(PO_4)_3$ was synthesized by a sol-gel method reported in a previous study [17]. First, 0.02 M $C_{16}H_{36}O_4Ti$ and 0.04 M $C_6H_8O_7$ were dissolved in a solution containing 280 mL H_2O_2 and 120 mL NH_4OH. Next, 0.13 M $NH_4H_2PO_4$ and 0.01 M Na_2CO_3 were dissolved in 80 mL DI water and 100 mL HNO_3, respectively. Then, the $NH_4H_2PO_4$ and Na_2CO_3 solutions were added into the solution containing $C_{16}H_{36}O_4Ti$ and $C_6H_8O_7$. The solution was aged at 140°C for 2 h to obtain a yellow precipitate and the resulting powder was annealed at 800°C for 12 h (ramp rate = 2°C min^{-1}). The $NaTi_2(PO_4)_3$ powder was ground with a mortar and pestle and was annealed again at 800°C for 12 h to improve the uniformity and crystallinity of the sample. The crystal structure and XRD pattern of $NaTi_2(PO_4)_3$ (space group: R-3c, a = b = 8.502 Å and c = 21.833 Å) are shown in Fig. S4.

NiHCF was synthesized by a co-precipitation method following the procedure reported in a previous study [41]. A 150 mL solution containing 0.10 M $Na_4Fe(CN)_6$ was slowly added into a 150 mL solution containing 0.10 M $NiCl_2$ and 0.70 M $Na_3C_6H_5O_7$. The resulting solution was stirred for 5 h and was then aged at room temperature for 20 h. A pale blue precipitate formed and was centrifuged at 5000 rpm, rinsing alternately with water and ethanol. Finally, the resulting precipitate was dried at 70°C for 24 h in a vacuum furnace held at a pressure of ~13.6 psi. The as-prepared NiHCF powder has a rhombohedral structure (space group: R-3, a = b = 7.389 Å and c = 17.310 Å) (Fig. S6a-b). The XRD pattern of NiHCF is also shown in Fig. S6c. The details of the structure are summarized in Table S1. EDS analysis reveals that the chemical formula of the as-prepared NiHCF powder is $Na_{1.20}Ni[Fe(CN)_6]_{0.85}$•$nH_2O$.

4.3. Preparation of sheet-type electrodes

The Bi, $NaTi_2(PO_4)_3$, and NiHCF electrodes used in this study were prepared through a ball milling process followed by a rolling-pressing procedure. The active material (Bi_2O_3, $NaTi_2(PO_4)_3$, or NiHCF) and graphite powder were first mixed with a mortar and pestle (the ratio of the active material to graphite powder was ~4:1 by mass), and then the mixture was ball milled for 1 h at a rate of 1060 cpm using a High-Energy Ball Mill (8000 M Mixer/Mill from SPEX SamplePrep). The resulting composite (Bi_2O_3/C, $NaTi_2(PO_4)_3$/C, or NiHCF/C) was mixed with a PTFE binder (ratio of ~1.6:1 by mass) using water as the solvent to form a thick slurry. The slurry was repeatedly kneaded, folded, and pressed using a mortar and pestle, followed by the use of a roll-press to form a thin sheet with desired dimensions. Finally, the electrode sheet was dried on a hot plate at 80°C for at least 6 h to remove water and residual organic compounds. The dried electrode sheet was cut into a 1 cm^2 electrode and was then attached onto a graphite current collector with carbon paint to perform electrochemical tests.

4.4. Characterization

The morphology and crystal structure of the active materials were examined using a LEO Supra55 VP Scanning Electron Microscope (SEM) at an accelerating voltage of 2 kV and powder X-ray diffractometer (XRD) (Bruker D8 Advanced PXRD, Ni-filtered Cu Kα radiation, λ = 1.5418 Å), respectively. Energy dispersive X-ray spectroscopy (EDS) was performed using the same SEM equipped with an EDS (Noran System Seven, Thermo Fisher) at an accelerating voltage of 12 kV. To investigate the phase change of the Bi electrode after oxidation (chlorination) and reduction (dechlorination), ex-situ XRD analysis was performed on the cycled samples.

4.5. Cyclability Tests

The cycle performances of all electrodes were examined in 0.6 M NaCl (salinity = 3.5%), which mimics the salinity of seawater (~3.5%). An undivided three-electrode cell was used, and the electrolyte was not circulated or stirred during the measurements. The cycle performance of the Bi electrode was examined galvanostatically at a current density of ± 4 mA cm^{-2} with cutoff potentials of −1.45 V and 0.7 V vs Ag/AgCl. The Bi electrode used as the working electrode (geometric area of 1 cm^2) contained ~6.9 mg of Bi. Thus, 4 mA cm^{-2} is equivalent to ~1.5 C-rate based on the theoretical capacity of 384.75 mAh g^{-1}. A NiHCF electrode (geometric area of 4 cm^2) was used as the counter electrode. The counter electrode had a sufficient amount of active material relative to the working electrode to ensure that the current flow was not limited by the counter electrode during the electrochemical tests. The cycle performance of the $NaTi_2(PO_4)_3$ electrode was examined galvanostatically at ± 2 mA cm^{-2} with cutoff potentials of −0.93 V and −0.2 V vs Ag/AgCl. The $NaTi_2(PO_4)_3$ electrode used as the working electrode (geometric area of 1 cm^2) contained ~10 mg of $NaTi_2(PO_4)_3$. Thus, ± 2 mA cm^{-2} is equivalent to ~1.5 C-rate based on the theoretical capacity of 133 mAh g^{-1}. A NiHCF electrode (geometric area of 4 cm^2) was used as the counter electrode. The cycle performance of the NiHCF electrode

was examined galvanostatically at ± 4 mA cm^{-2} with cutoff potentials of 0.0 V and 0.9 V vs Ag/AgCl. The NiHCF electrode used as the working electrode (geometric area of 1 cm^2) contained ~11 mg of NiHCF. As the exact theoretical capacity of NiHCF cannot be accurately determined because of the water content that varies with temperature and humidity, 60 mA g^{-1} was used as 1 C-rate in this study, which is a common assumption made in the studies of PBA-based Na-storage electrodes [37]. Thus, ± 4 mA cm^{-2} is equivalent to ~ 6 C-rate. A BiOCl electrode (geometric area of 4 cm^2) was used as the counter electrode. For all experiments, an Ag/AgCl (4 M KCl) reference electrode was placed near the working electrode to monitor the potential change of the working electrode during the cyclability tests.

4.6. Operation of Charging and Discharging Cells

The operation of Charging Cell 1 composed of a $NaTi_2(PO_4)_3$ electrode (geometric area of 4 cm^2) and a Bi electrode (geometric area of 1 cm^2) was galvanostatically tested in 0.6 M NaCl at 1.33 mA cm^{-2} (~0.5 C-rate based on the Bi electrode) until the capacity of the Bi electrode reached 100 mAh g^{-1}. When the operation of Charging Cell 1 was complete, the Bi/BiOCl electrode was manually lifted from the solution, rinsed with DI water, and then moved to Charging Cell 2. In Charging Cell 2, the Bi/BiOCl electrode and a fully desodiated NiHCF electrode (geometric area of 4 cm^2) were electrically connected and immersed in 70 mM HCl (pH 1.3). Then, Charging Cell 2 was galvanostatically operated at 1.33 mA cm^{-2} until the potential of the Bi/BiOCl electrode reached −0.4 V vs Ag/AgCl. When the operation of Charging Cell 2 was complete, the NiHCF electrode from Charging Cell 2 and the $NaTi_2(PO_4)_3$ electrode from Charging Cell 1 were moved to Discharging Cell. These two electrodes were electrically connected and immersed in a 0.6 M NaCl solution. Discharging Cell was operated at a constant current of 1.33 mA cm^{-2} until the potential of the NiHCF electrode reached 0.15 V vs Ag/AgCl. In all experiments, the Ag/AgCl (4 M KCl) reference electrode was placed between the working electrode and the counter electrode to monitor changes in the individual potentials of both electrodes.

The Coulombic efficiency of the Bi electrode is ~104%, meaning that its dechlorination capacity is higher than its chlorination capacity. The capacities of Charging Cell 1 (100 mAh $g_{Bi}{}^{-1}$) and Charging Cell 2 (105.29 mAh $g_{Bi}{}^{-1}$) shown in Fig. S10a-b were determined based on the chlorination and dechlorination capacities of Bi, respectively. (The $NaTi_2(PO_4)_3$ and NiHCF electrodes used in this study contained excess $NaTi_2(PO_4)_3$ and NiHCF, respectively, and their total electrode capacities were much greater than that of Bi.) Therefore, the sodiation capacity of $NaTi_2(PO_4)_3$ during the operation of Charging Cell 1 was less than the desodiation capacity of NiHCF during the operation of Charging Cell 2. When sodiated $NaTi_2(PO_4)_3$ and desodiated NiHCF were combined in Discharging Cell, the cell operation continued until NiHCF regained the same amount of Na^+ that it had released in Charging Cell 2 (105.36 mAh $g_{Bi}{}^{-1}$). Thus, the desodiation capacity of $NaTi_2(PO_4)_3$ in Discharging Cell was greater than the sodiation capacity of $NaTi_2(PO_4)_3$ in Charging Cell 1. Because the initial $NaTi_2(PO_4)_3$ electrode used in Charging Cell 1 was pre-sodiated and contained excess $Na_3Ti_2(PO_4)_3$, this discrepancy could be tolerated for a few cycles. However, when necessary, the $NaTi_2(PO_4)_3$ electrode was additionally sodiated to maintain the Na^+ content in the electrode as ~30% of its capacity.

Another major effect of the capacity of Discharging Cell being greater than that of Charging Cell 1 is that it leads to an overestimated energy output and therefore an overestimated energy efficiency. (The energy output (input) is the product of the capacity and output (input) voltage.) Thus, in order to obtain a more accurate energy efficiency, which would have been obtained if the Coulombic efficiency of the Bi electrode was 100%, we normalized the capacities of all three cells to be identical (100 mAh). The results using normalized capacities are shown in Fig. 4. and results obtained using the as-obtained capacities are shown in Fig. S10.

4.7. Determination of Na^+ and Cl^- removal efficiencies

The actual concentrations of Na^+ and Cl^- present in the electrolyte of Charging Cell 1 were measured by a sodium ion meter (Horiba B-722) and a chloride ion meter (Horiba 6560-10C) after passing a charge of 0, 9, 18, and 27 C. An undivided three-electrode cell consisting of a Bi electrode as the working electrode, a $NaTi_2(PO_4)_3$ electrode as the counter electrode, and an Ag/AgCl electrode (4 M KCl) as the reference electrode was used for this experiment. A constant potential of 0.6 V vs. Ag/AgCl was applied to oxidize Bi to BiOCl. As the size of the Bi electrode in this experiment was limited, a 0.06 M NaCl solution was used to ensure that reliable changes in the Na^+ and Cl^- concentrations were measured by the sodium and chloride ion meters. For the chloride ion meter whose accuracy is considerably affected by the conductivity of the sample solution, 0.1 M KNO_3 was added to the sample solution to provide optimum solution conductivity. The FE for ion removal was determined by dividing the measured ion concentration by the theoretically expected ion concentration based on the charge passed. The resulting value was multiplied by 100% and is reported as a percentage.

Declaration of competing interest

There are no conflicts to declare.

Acknowledgements

This work was supported by the National Science Foundation (NSF) through grants CBET-1803496 and PFI-2016321 and the Draper Technology Innovation Fund (University of Wisconsin-Madison).

Supplementary materials

Supplementary material associated with this article can be found, in the online version, at doi:10.1016/j.ensm.2021.02.037.

References

[1] P.A. Owusu, S. Asumadu-Sarkodie, A review of renewable energy sources, sustainability issues and climate change mitigation, Cogent. Eng. 3 (2016) 1167990.
[2] B. Dunn, H. Kamath, J.–M Tarascon, Electrical energy storage for the grid: A battery of choices, Science 334 (2011) 928–935.
[3] Z. Yang, J. Zhang, M.C.W. Kintner-Meyer, X. Lu, D. Choi, J.P. Lemmon, J. Liu, Electrochemical energy storage for green grid, Chem. Rev. 111 (2011) 3577–3613.
[4] R.C. Armstrong, C. Wolfram, K.P. de Jong, R. Gross, N.S. Lewis, B. Boardman, A.J. Ragauskas, K. Ehrhardt-Martinez, G. Crabtree, M.V. Ramana, The frontiers of energy, Nat. Energy 1 (2016) 15020.
[5] B. Zakeri, S. Syri, Electrical energy storage systems: A comparative life cycle cost analysis, Renew. Sustain. Energy Rev. 42 (2015) 569–596.
[6] Y. Kim, G.–T. Kim, S. Jeong, X. Dou, C. Geng, Y. Kim, S. Passerini, Large-scale stationary energy storage: Seawater batteries with high rate and reversible performance, Energy Storage Mater. 16 (2019) 56–64.
[7] J.B. Goodenough, K.-S. Park, The Li-ion rechargeable battery: A perspective, J. Am. Chem. Soc 135 (2013) 1167–1176.
[8] D. Lin, Y. Liu, Y. Cui, Reviving the lithium metal anode for high-energy batteries, Nat. Nanotech. 12 (2017) 194–206.
[9] M. Ko, S. Chae, J. Ma, N. Kim, H.-W. Lee, Y. Cui, J. Cho, Scalable synthesis of silicon–nanolayer-embedded graphite for high-energy lithium-ion batteries, Nat. Energy 1 (2016) 16113.
[10] L. Lu, X. Han, J. Li, J. Hua, M. Ouyang, A review on the key issues for lithium-ion battery management in electric vehicles, J. Power Sources 226 (2013) 272–288.
[11] H. Kim, J. Hong, K.–Y. Park, H. Kim, S.–W. Kim, K. Kang, Aqueous rechargeable Li and Na ion batteries, Chem. Rev. 114 (2014) 11788–11827.
[12] D. Bin, F. Wang, A.G. Tamirat, L. Suo, Y. Wang, C. Wang, Y. Xia, Progress in aqueous rechargeable sodium-ion batteries, Adv. Energy Mater. 8 (2018) 1703008.
[13] J. Shin, J.W. Choi, Opportunities and reality of aqueous rechargeable batteries, Adv. Energy Mater. 10 (2020) 2001386.
[14] D. Kundu, E. Talaie, V. Duffort, L.F. Nazar, The emerging chemistry of sodium ion batteries for electrochemical energy storage, Angew. Chem., Int. Ed. 54 (2015) 3431–3448.
[15] C. Vaalma, D. Buchholz, M. Weil, S. Passerini, A cost and resource analysis of sodium-ion batteries, Nat. Rev. Mater. 3 (2018) 18013.
[16] M. Pasta, C.D. Wessells, Y. Cui, F.L. Mantia, A desalination battery, Nano Lett. 12 (2012) 839–843.
[17] D.–H. Nam, K.–S. Choi, Bismuth as a new chloride-storage electrode enabling the construction of a practical high capacity desalination battery, J. Am. Chem. Soc. 139 (2017) 11055–11063.

[18] F. Chen, Y. Huang, L. Guo, L. Sun, Y. Wang, H.Y. Yang, Dual-ions electrochemical deionization: a desalination generator, Energy Environ. Sci. 10 (2017) 2081–2089.
[19] S. Kim, H. Yoon, D. Shin, J. Lee, J. Yoon, Electrochemical selective ion separation in capacitive deionization with sodium manganese oxide, J. Colloid Interface Sci. 506 (2017) 644–648.
[20] F. Chen, Y. Huang, L. Guo, M. Ding, H.Y. Yang, A dual-ion electrochemistry deionization system based on AgCl-$Na_{0.44}MnO_2$ electrodes, Nanoscale 9 (2017) 10101–10108.
[21] W. Zhao, L. Guo, M. Ding, Y. Huang, H.Y. Yang, Ultrahigh desalination-capacity dual-ion electrochemical deionization device based on $Na_3V_2(PO_4)_3$@C–AgCl electrodes, ACS Appl. Mater. Interfaces 10 (2018) 40540–40548.
[22] L. Wang, C. Mu, H. Li, F. Li, A dual-function battery for desalination and energy storage, Inorg. Chem. Front. 5 (2018) 2522–2526.
[23] F. Chen, Y. Huang, D. Kong, M. Ding, S. Huang, H.Y. Yang, $NaTi_2(PO_4)_3$-Ag electrodes based desalination battery and energy recovery, FlatChem 8 (2018) 9–16.
[24] D.–H. Nam, M.A. Lumley, K.–S. Choi, A desalination battery combining $Cu_3[Fe(CN)_6]_2$ as a na-storage electrode and Bi as a Cl-storage electrode enabling membrane-free desalination, Chem. Mater. 31 (2019) 1460–1468.
[25] Y.X. Huang, F. Chen, L. Guo, J. Zhang, T.P. Chen, H.Y. Yang, Low energy consumption dual-ion electrochemical deionization system using $NaTi_2(PO_4)_3$–AgNPs electrodes, Desalination 451 (2019) 241–247.
[26] M. Suss, V. Presser, Water desalination with energy storage electrode materials, Joule 2 (2018) 10–15.
[27] P. Srimuk, X. Su, J. Yoon, D. Aurbach, V. Presser, Charge transfer materials for electrochemical water desalination, ion separation and the recovery of elements, Nat. Rev. Mater. 5 (2020) 517–538.
[28] D.–H. Nam, M.A. Lumley, K.–S. Choi, Electrochemical redox cells capable of desalination and energy storage: Addressing challenges of the water–energy nexus, ACS Energy Lett. 6 (2021) 1034–1044.
[29] Z. Li, D. Young, K. Xiang, W.C. Carter, Y.–M. Chiang, Towards high power high energy aqueous sodium-ion batteries: The $NaTi_2(PO_4)_3$/$Na_{0.44}MnO_2$ system, Adv. Energy. Mater. 3 (2013) 290–294.
[30] H. Kabbour, D. Coillot, M. Colmont, C. Masquelier, O. Mentré, A-$Na_3M_2(PO_4)_3$ (M = Ti, Fe): Absolute cationic ordering in NASICON-type phases, J. Am. Chem. Soc. 133 (2011) 11900–11903.
[31] S.I. Park, I. Gocheva, S. Okada, J.–I Yamaki, Electrochemical properties of $NaTi_2(PO_4)_3$ anode for rechargeable aqueous sodium-ion batteries, J. Electrochem. Soc. 158 (2011) A1067–A1070.
[32] Z. Li, D.B. Ravnsbæk, K. Xiang, Y.–M. Chiang, $Na_3Ti_2(PO_4)_3$ as a sodium-bearing anode for rechargeable aqueous sodium-ion batteries, Electrochem. Commun. 44 (2014) 12–15.
[33] D.–H. Nam, K.–S. Choi, Electrochemical desalination using Bi/BiOCl electrodialysis cells, ACS Sustainable Chem. Eng. 6 (2018) 15455–15462.
[34] D.–H. Nam, D. Lee, K.–S. Choi, Electrochemical and photoelectrochemical approaches for the selective removal, recovery, and valorization of chloride ions, Chem. Eng. J. 404 (2021) 126378.
[35] S. Burn, M. Hoang, D. Zarzo, F. Olewniak, E. Campos, B. Bolto, O. Barron, Desalination techniques - a review of the opportunities for desalination in agriculture, Desalination 364 (2015) 2–16.
[36] C. Fritzmann, J. Löwenberg, T. Wintgens, T. Melin, State-of the-art of reverse osmosis desalination, Desalination 216 (2007) 1–76.
[37] C.D. Wessells, S.V. Peddada, R.A. Huggins, Y. Cui, Nickel hexacyanoferrate nanoparticle electrodes for aqueous sodium and potassium ion batteries, Nano Lett. 11 (2011) 5421–5425.
[38] H.–W. Lee, M. Pasta, R.Y. Wang, R. Ruffo, Y. Cui, Effect of the alkali insertion ion on the electrochemical properties of nickel hexacyanoferrate electrodes, Faraday Discuss. 176 (2014) 69–81.
[39] B. Wang, Y. Han, X. Wang, N. Bahlawane, H. Pan, M. Yan, Y. Jiang, Prussian blue analogs for rechargeable batteries, iScience 3 (2018) 110–133.
[40] J. Lee, S. Kim, J. Yoon, Rocking chair desalination battery based on Prussian blue electrodes, ACS Omega 2 (2017) 1653–1659.
[41] M.A. Lumley, D.–H. Nam, K.–S. Choi, Elucidating structure-composition-property relationships of Ni-based Prussian blue analogues for electrochemical seawater desalination, ACS Appl. Mater. Interfaces 12 (2020) 36014–36025.
[42] A.I. Mohamed, N.J. Sansone, B. Kuei, N.R. Washburn, J.E. Whitacre, Using polypyrrole coating to improve cycling stability of $NaTi_2(PO_4)_3$ as an aqueous Na-ion anode, J. Electrochem. Soc. 162 (2015) A2201–A2207.
[43] R.K.B. Karlsson, A. Cornell, Selectivity between oxygen and chlorine evolution in the chlor-alkali and chlorate processes, Chem. Rev. 116 (2016) 2982–3028.
[44] I. C. Watson, O. J. Morin, L. Henthorne, Desalting Handbook for Planners, 3rd Ed. 72; United States Department of the Interior Bureau of Reclamation; 2003.